Chinese Journal of
POLYMER SCIENCE

RESEARCH ARTICLE

https://doi.org/10.1007/s10118-023-2939-x
Chinese J. Polym. Sci. **2023**, *41*, 811–823

Control Aggregation of P3HT in Solution for High Efficiency Doping: Ensuring Structural Order and the Distribution of Dopants

Duo Liu[a,b], Jun-Hang Li[a,b], Si-Chun Wang[a,b], Lu Zhang[a,b], Xin-Yu Liu[a,b], Qiang Zhang[a*], and Yan-Chun Han[a,b*]

[a] *State Key Laboratory of Polymer Physics and Chemistry, Changchun Institute of Applied Chemistry, Chinese Academy of Sciences, Changchun 130022, China*
[b] *School of Applied Chemistry and Engineering, University of Science and Technology of China, Hefei 230026, China*

Electronic Supplementary Information

Abstract Molecular doping is one of the most important tools to manipulate the electrical properties of conjugated polymers for application in organic optoelectronics. The polymer crystallinity and distribution position of the dopant crucially determine electrical conductivity of the doped polymer. However, in solution-mixed doping, the interplay between polymer and dopant leads to highly structural disorder of polymer and random arrangement of dopant. Here, we propose a strategy to ensure the dopant induced polarons have high charge dissociation and transport by letting the conjugated polymers aggregate in the marginal solvent solution by cooling it from higher temperature to room temperature. We select poly(3-hexylthiophene-2,5-diyl) (P3HT) solution doped by 2,3,5,6-tetrafluoro-7,7,8,8-tetracyanoquinodimethane (F4TCNQ) as a model system. P3HT crystallizes in the marginal solvent, such as 1,1,2-trichloroethane (TCE) driven by the favor π-π interaction between planar polymer backbone. The dopant F4TCNQ enters the alkyl side chain region not the π-π stacking region and thus guarantees high crystallinity and the π-π interaction of P3HT. This distribution of F4TCNQ which away from the polymer backbone to ensure higher charge dissociation and transport. Finally, we obtained a high conductivity value of 23 S/cm by doping P3HT with 20% F4TCNQ by using the marginal solvent, which is higher than doping P3HT with a disordered coil conformation in chlorobenzene (CB) of 7 S/cm, which the dopants enter both the alkyl side chain region and the π-π stacking region.

Keywords Solvent; Crystalline; Dopant location; Doping efficiency; Electrical conductivity

Citation: Liu, D.; Li, J. H.; Wang, S. C.; Zhang, L.; Liu, X. Y.; Zhang, Q.; Han, Y. C. Control aggregation of P3HT in solution for high efficiency doping: ensuring structural order and the distribution of dopants. *Chinese J. Polym. Sci.* **2023**, *41*, 811–823.

INTRODUCTION

Chemical doping is a feasible way to improve conductivity and change Fermi level of conjugated semiconductor polymers for application in organic optoelectronics.[1,2] In general, for chemical doping, it involves the addition of an electron acceptor or electron donor in conjugated polymer for P- or N-type doping, respectively.[1] For the P-type doping, the doping mechanism is that the electrons from the highest occupied energy level (HOMO) of conjugated polymer transfer to the lowest unoccupied energy level (LUMO) of the molecular dopant.[3] In the doped conjugated polymer literature, when polymers are mixed with dopant, the integer charge transfer (ICT) appears to dominate doping process while small molecules are mixed with dopant mainly form charge transfer complex (CTC). The process of ICT and CTC is shown in Scheme 1.

* Corresponding authors, E-mail: zhqawh@ciac.ac.cn (Q.Z.)
E-mail: ychan@ciac.ac.cn (Y.C.H.)

Special Issue: In Memory of Professor Fosong Wang
Received November 26, 2022; Accepted December 26, 2022; Published online March 2, 2023

The simplest method of molecular doping is to mix conjugated polymer solution with dopant solution to tune the doping level by adding different dopant concentrations. Moreover, solution-mixed doping can fabricate different thick conducting polymer films with homogeneous doping level and be compatible with various large-scale processing techniques. Although some semiconducting polymers have been successfully doped by using solution-mixed method, the electrical conductivity is still much lower than those by evaporation doping and solution sequential doping methods.[4–7] Therefore, an understanding of the solution doping process and how the conformation and aggregation of polymers in the solution affect doping are needed to further investigation.[8,9] It is known that the solubility of many polymers will be reduced by the addition of the dopant to form undesired structures in solution-mixed doping which cause low electrical conductivity (generally below 10^1 S/cm).[4,10,11] Another very critical issue is the way in which dopants are distributed in final thin films which is important to the efficiency of free-carrier formation and it also has a big effect on the conductivity of the doped polymer. In solution-mixed doping, the complicated interaction between dopants with polymer chain causes dopants to distribute disorderly in the crystal-

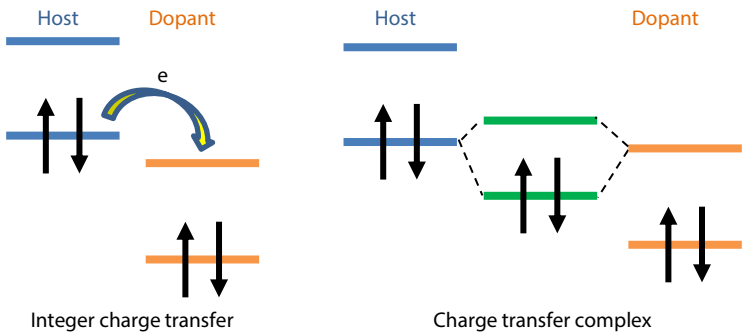

Scheme 1 Two doping mechanisms in molecular doping: integer charge transfer (ICT) and charge transfer complex (CTC).

line region, amorphous region, π-π region and lamellar region of polymer film.[11,12] The ideal distribution of dopant is in the lamellar region of polymer and this is because the polarons on the polymer chain and the dopant counterions are far apart, which facilitates the rapid delocalization and transport of charge. This location is especially important when dealing with semiconductor polymer which has low dielectric constant.

P3HT doped with F4TCNQ is a model system to investigate the correlation between structure, charge transport and electrical properties.[10,11,13–15] In general, P3HT and F4TCNQ mainly undergo integer charge transfer process and then follow charge separation and transport.[16–19] Many factors affect charge separation and transport, including the crystallinity of the polymer, the distance between dopant and polymer chain, the DOS distribution, and so on.[15] The addition of F4TCNQ will greatly accelerate the aggregation rate of P3HT in solution. P3HT aggregates have faster reaction rate with F4TCNQ which is a result of faster charge delocalization after the charge transfer process.[20–22] The type of P3HT aggregates can also affect the doping process. The J- and H-type aggregates of P3HT can be produced by using solvent toluene and anisole. After doping with F4TCNQ, the J-type aggregates exhibit a higher doping efficiency compared to the H-type aggregates.[23] Although an efficient and rapid doping process can occur between P3HT and F4TCNQ, the most of carriers remain strongly bound and only 5% dissociate and transport.[3] It is shown that a new crystalline phase will be formed between P3HT and F4TCNQ with dopants interacting with side region and π-π region simultaneously after solution-mixed doping.[11,12,14,24,25] However, the dopant remaining in π-π region of polymer is not ideal, which has a close distance with backbone. It will cause the localization of the charge and destroy the charge separation and damage the charge transport channel. Therefore, in solution-mix doping, it is not easy to achieve efficient doping, both ensuring the structure order of the film and controlling the distribution of dopants.

In the present work, in order to investigate the correlation between solution state and electrical properties, we controlled P3HT solution state by selecting two different kinds of solvents, marginal solvent TCE and good solvent CB. We then controlled the producing of aggregates and disordered coil conformation in solution by cooling the solution from higher temperature to room temperature. After doping with F4TCNQ, we obtained two kinds of doping stacking structures. When the P3HT aggregates in TCE were doped, the dopant was only distributed in the alkyl side chain region of the polymer. When P3HT doped in CB, the dopant entered the alkyl side chain region and π-π region of the polymer which is not conducive to the charge separation and transport in doped polymer. Finally, we obtained a high conductivity value of 23 S/cm by doping P3HT with 20% F4TCNQ by using the marginal solvent, which is higher than doping P3HT with a disordered coil conformation in CB (7 S/cm).

EXPERIMENTAL

Materials

Poly(3-hexylthiophene-2,5-diyl) (P3HT, M_n=35.2 kg/mol, PDI=2.1, regioregularity=97.3%) was purchased from Ossila (UK). Dopant 2,3,5,6-tetrafluoro-7,7,8,8-tetracyanoquinodimethane (F4TCNQ, purified by sublimation, purity >98.0%) was purchased from TCI (Shanghai, China). Solvent chlorobenzene (CB, purity >99%), 1,1,2-trichloroethane (TCE, purity >99%), 1,2,4-trichlorobenzene (TCB, purity >99%), acetonitrile (ACN, purity >99%), 2-chlorophenol (2-CP, purity >99%), and heptane (Hep, purity >99%) were purchased from Macklin (Shanghai, China). All solvents were used as received without further purification.

Sample Preparation

Neat P3HT solutions of 1 mg/mL were prepared by dissolving P3HT in either CB or TCE and heated to 100 °C for 3 h to dissolve completely, then slowly cooled to room temperature with a rate of 25 °C/h. F4TCNQ was dissolved in both CB and TCE solvents at a concentration of 1 mg/mL and heated to 100 °C for 5 h to dissolve completely. The doping process was done by mixing P3HT solution and F4TCNQ solution in the same solvent by adding different weight amounts of F4TCNQ at room temperature. Thin films were drop-coated from the doping solution onto cleaned glass substrates. Substrates were sequentially sonicated for 15 min in acetone, isopropyl alcohol and deionized water and finally blown dry with nitrogen. The thickness of film was about 300 nm measured by Veeco Dektak 150 Profilometer.

UV-Vis-NIR Absorption Spectroscopy

The UV-Vis-NIR absorption data was obtained from the AvaSpec-3648 spectrometer (Avantes, Netherlands). The measurements were carried out within a wavelength range of 300–1000 nm. The solution sample was placed in a 2 mm thick quartz cuvette and tested. The neat P3HT solution concentration was 1 mg/mL, and the dopant concentration in

https://doi.org/10.1007/s10118-023-2939-x

the doped polymer solution was 5 wt%, 10 wt%, 15 wt%, 20 wt%, 25 wt% and 30 wt%, respectively. The UV-Vis absorption measurements were taken at room temperature.

Dynamic Light Scattering (DLS)

The DLS experiment of P3HT solution was performed using a light scattering goniometer (BI200-SM, Brookhaven Instruments) equipped with a digital autocorrelator (BI-9000 AT, Brookhaven Instruments) and an Ar ion laser (Model 95, Lexel Laser, Inc.).[26] The solution sample was placed in a 5 mm thick quartz cuvette and tested and the pristine P3HT solution concentration was 1 mg/mL in both TCE and CB. The DLS measurements were taken at room temperature.

FTIR Spectroscopy

Doped P3HT films FTIR spectra were collected by using a Bruker spectrometer (ALPHA) on KBr substrates. Signal of thin film sample was recorded in the atmosphere. Using a transmission module to test the samples and obtain high signal-to-noise ratio data of vibrational absorption peak of cyano group.

Grazing Incidence X-Ray Diffraction (GIXRD) and Two-Dimensional Grazing Incidence Wide Angle X-Ray Scattering (2D GIWAXS)

Out-of-plane GIXRD data was obtained on a Bruker D8 Discover Reflector (Cu Kα, λ=1.54 Å) with 40 kV and 40 mA tube current. In-plane GIXRD was performed on a Rigaku SmartLab X-ray diffractometer (Cu Kα, λ=1.54 Å). Both out-of-plane GIXRD data and in-plane GIXRD data were obtained from a scanning region of 2θ between 2° and 30°. 2D GIWAXS tests were obtained at the 1W1A beamline of Beijing Synchrotron Radiation Facility (BSRF) (λ=1.54 Å). The incidence angle is 0.16° and the exposure time of samples is 400 s.

Transmission Electron Microscopy (TEM) and Cryogenic Transmission Electron Microscopy (Cryo-TEM)

The TEM images of film were acquired using a JEM-1400 microscope (JEOL, Japan) operated at 120 kV. The cryo-TEM images of solution were obtained by using a JEM-3200FSC microscope (JEOL, Japan) operated at 300 kV and with a Gatan charge-coupled device camera. For sample preparation, a small droplet of P3HT solution sample was dropped onto a copper grid with holey carbon film. And then the sample was quickly inserted into liquid nitrogen for cooling. After waiting 10 min, the sample was transferred to sample warehouse of JEM-3200FSC microscope. The magnification of the images was 120,000 times and exposure time was 1 s.

Cryogenic Scanning Electron Microscopy (Cryo-SEM)

Cryo-SEM analysis was performed on Sigma 300 microscope (ZEISS, Germany). Sample solution (10 μL) was dropped onto a sample stage and then quickly inserted into liquid nitrogen for cooling for a few seconds. The frozen sample was transferred to the preparation chamber where it was cut to create a new section. To remove the solvent from the frozen sample, the sample was sublimated at −80 °C for 30 min. Finally, the sample was gilded and scanned with electron beam. Cryo-SEM images were obtained by a low electron detector with accelerating voltage of 5.0 kV and at temperature of −130 °C.

Conductivity Measurements

The electrical conductivity was measured by the four-probe method. By thermal evaporation with specific shadow mask, gold was deposited on the surface of the samples and formed four channels (40 nm thick) on the surface of the samples. The length of the channel was 1 mm and the width was 0.2 mm and the distance between adjacent channels was 0.2 mm. The electrical conductivity data can be calculated by the following formula: $\sigma = Iw/Vld$. In the formula, σ is the electrical conductivity, V is the voltage, I is the current, l is the length of channel, w is the width of channel and d is the thickness of film. Five data were averaged for each doping concentration.

RESULTS AND DISCUSSION

Electrical Properties

We chose P3HT/F4TCNQ system to investigate the correlation between solution state and electrical properties. The chemical structures of host P3HT, dopant F4TCNQ and solvents of TCE and CB are shown in Fig. 1(a). The P3HT solutions of 1 mg/mL were prepared by dissolving P3HT in either TCE or CB and heated to 100 °C for 3 h, then slowly cooled to room temperature at a rate of 25 °C/h. F4TCNQ was dissolved in either TCE or CB at a concentration of 1 mg/mL and heated to 100 °C for 5 h. The doping process was done by mixing P3HT solution and F4TCNQ solution in the same solvent with adding different weight amounts of F4TCNQ at room temperature. The HOMO and LUMO levels of P3HT and F4TCNQ are −4.8 and −2.7 eV, −8.3 eV and −5.2 eV, respectively.[27,28] The LUMO level of F4TCNQ is lower than HOMO level of P3HT which is the basis of ground state of charge transfer process. The effects of adding F4TCNQ on the electrical conductivity of the P3HT thin films were studied based on four-point probe method. Five data were averaged for each doping concentration (Table S1a in the electronic supplementary information, ESI). Fig. 1(b) is the plots of the electrical conductivities of P3HT doped with various concentrations of F4TCNQ from solvent TCE and CB. The pristine film of P3HT showed electrical conductivity of $2.6\times10^{-4}\pm 5.7\times10^{-5}$ S/cm processed from TCE which was higher than electrical conductivity of $8.5\times10^{-5}\pm1.3\times10^{-5}$ S/cm processed from CB. Upon mixing with F4TCNQ, the conductivity of P3HT doped F4TCNQ processed from TCE rapidly increased, reached the maximum electrical conductivity of 23.0±0.5 S/cm with 20 wt% F4TCNQ loading and decreased upon further addition of dopant. The maximum electrical conductivity of F4TCNQ doped P3HT processed from CB was 7.0±0.2 S/cm with 20 wt% F4TCNQ loading. In the whole region, F4TCNQ doped P3HT processed from TCE has a higher electrical conductivity compared to F4TCNQ doped P3HT processed from CB, and the maximum difference is about 40 times as shown in Fig. 1(c). When the dopants concentration exceeded 15 wt%, the difference of electrical conductivity between TCE and CB stabilized at about 3 times.

The doping efficiency and electrical conductivity are closely related to the doping method and experimental conditions. There are many studies on the doping process of P3HT/F4TCNQ system and the electrical conductivity reported also shows great differences.[5–7,11,13,14,29] Table S1(b) (in ESI) lists the electrical conductivity reported previously by solution-mixed doping.[10,11,13,17,20,29–34] In the solution-mixed doping, the most common used solvents are chloroform and chlorobenzene. Besides, the electrical conductivity obtained

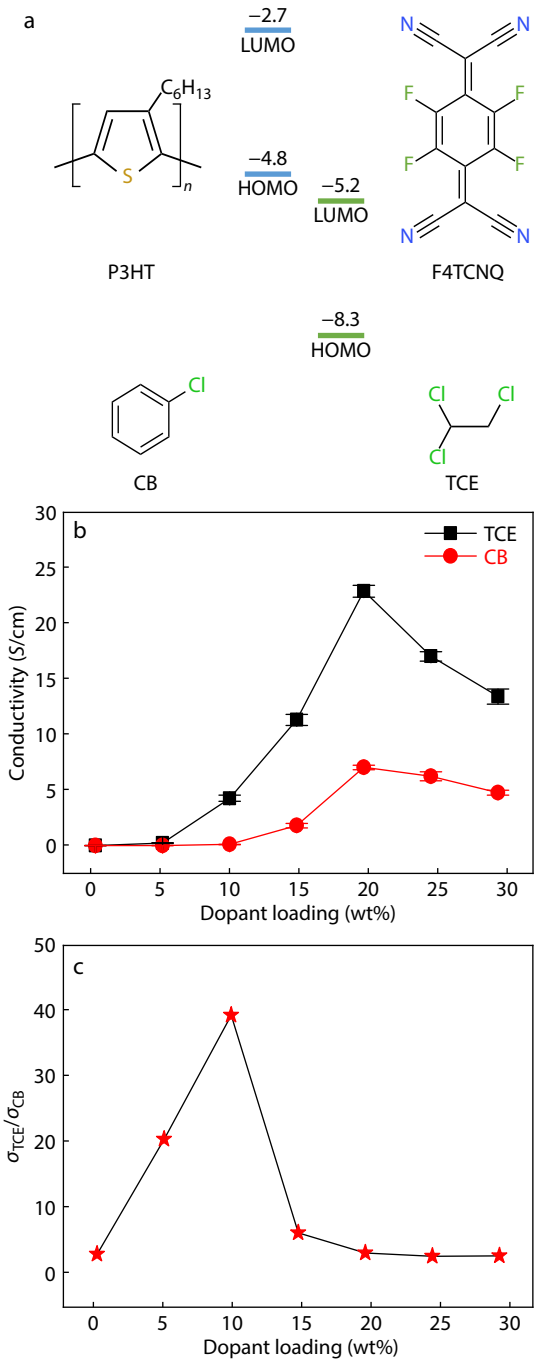

Fig. 1 (a) Chemical structures of host P3HT and dopant F4TCNQ with the position of HOMO and LUMO of P3HT and F4TCNQ and solvents of TCE and CB, respectively; (b) Evolution of electrical conductivity of doped P3HT as a function of F4TCNQ concentration. The content of dopant was the mass ratio between F4TCNQ and P3HT. The red line represented processing from solvent TCE and the black line represented processing from solvent CB. (c) Ratio of electrical conductivity of doped P3HT processed from solvent TCE and CB as a function of F4TCNQ concentration.

by these solvents is usually very low which is in the level of 10^{-1}–10^{0} S/cm. In our work, the conductivity of P3HT doped F4TCNQ processed from TCE exceeded all previously reported values by solution-mixed doping.

A General Picture of High Doping Efficiency in Solvent TCE

From the above discussion, we can see that a high conductivity value of 23 S/cm by doping P3HT with 20% F4TCNQ by using the marginal solvent (TCE) is obtained, which is higher than doping P3HT in a good solvent chlorobenzene (CB) (7 S/cm). In order to explain the P3HT solution state on the conductivity, we investigate the UV-Vis-NIR absorbance spectra of P3HT solution, hydrodynamic diameter Rh by dynamic light scattering (DLS) and Cryo-SEM and TEM experiments.

The Hansen solubility parameter (HSP) is used to predict if a polymer can dissolve in a given solvent.[35,36] We tested the HSP of P3HT in different solvents using binary solvent gradient method (the details are listed in ESI, part 2). The three components of HSP of P3HT were δ_D=18.9 MPa$^{1/2}$, δ_p=3.4 MPa$^{1/2}$, and δ_H=3.0 MPa$^{1/2}$ with a radius of R_0=4.1 MPa$^{1/2}$ (Fig. 2a). The Ra value between P3HT and CB is 1.4, which means CB is a good solvent for P3HT. The Ra value between P3HT and TCE is 4.5, which means TCE is a marginal solvent for P3HT. By using the good solvent CB and the marginal solvent TCE, P3HT can be controlled to be dissolved or crystallized in the solution by temperature manipulation. Figs. 2(b) and 2(c) show the UV-Vis-NIR absorbance spectra of P3HT solution under different temperatures. The dissolution of P3HT in good solvent and marginal solvent produced a transparent orange solution at high temperature. But during cooling and ageing, the solution of P3HT in solvent TCE displayed a dramatic color change, from orange to dark brown which means P3HT crystallization in solution state by the driving force of π-π stacking, as shown in Fig. 2(b). However, in solvent CB, the UV-Vis-NIR absorbance spectra are kept unchanged. At room temperature, there are three distinct characteristic absorption peaks in the solution UV-Vis-NIR absorbance spectra of TCE, which are located at 605 nm, 557 nm and 520 nm, corresponding to the (0-0), (0-1) and (0-2) peaks of P3HT, respectively. At high temperature, there is only one absorption peak at 480 nm in TCE, and the same absorption peak occurs in CB which has nothing to do with temperature. From high temperature to low temperature, the π-π^* absorption peak of P3HT in TCE shifts from 480 nm to 520 nm with a redshift of 40 nm, which indicates that the backbone in solution has a more planar conformation and the conjugation length increases.[37–39] The presence of (0-0) peak and (0-1) peak also indicates the presence of ordered aggregates in the solution due to π-π interactions between the more planar polymer chains.

Furthermore, evidence about aggregation for P3HT/TCE solution was analyzed by using DLS, as shown in Fig. 3(a). The curve with two peaks from TCE suggests the coexistence of two P3HT phases with different size in P3HT/TCE solution. The smaller size with 11.7 nm representing the random coils of P3HT and the bigger size with 91.3 nm representing the crystallites of P3HT, respectively. But there is only one peak in P3HT/CB solution with size of 24.4 nm, and the P3HT chains dissolve entirely in CB which have greater random coils than the 11.7 nm in TCE. We also took high-resolution Cryo-TEM experiments to investigate the P3HT chains behavior in solution. In Fig. 3(b), the lamellar stacking of polymer along backbone can be seen clearly. And there is a superposition of

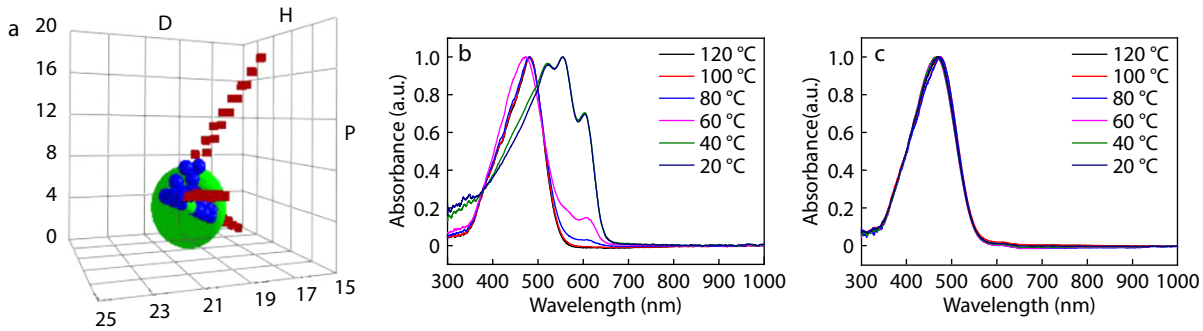

Fig. 2 (a) The HSP sphere of P3HT with central coordinate at (18.9, 3.4, 3.0) $MPa^{1/2}$ with the radius of the HSP sphere is R_0=4.1 $MPa^{1/2}$. UV-Vis-NIR absorbance spectra of P3HT solution in the solvent (b) TCE and (c) CB at different temperatures.

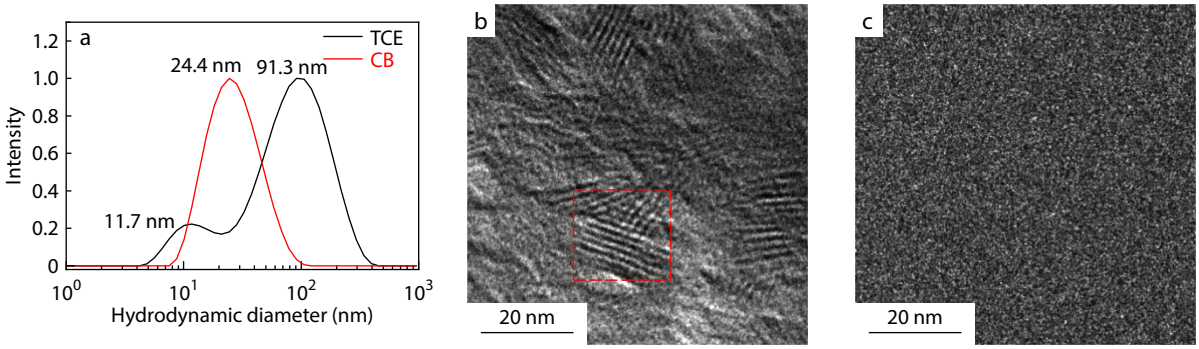

Fig. 3 (a) DLS of P3HT solution in the solvent TCE and CB. Cryo-TEM images of P3HT solution in the solvent (b) TCE and (c) CB.

lamellae in which polymer with different orientation. We can conclude that P3HT chain crystallization in TCE, but there is no obvious lamellar stacking in CB as shown in Fig. 3(c).

To explore the solution state of doping process, UV-Vis-NIR absorption spectra of undoped and doped P3HT solution are shown in Fig. 4. For P3HT doped with F4TCNQ, three new absorption peaks of the dopant anion appear in the spectrum, which are 413, 770 and 870 nm.[40] TCE solution of pristine P3HT shows a clear vibronic structure compared to CB solution, pointing to more ordered structure from TCE. After doping with F4TCNQ, the peak of neural P3HT is bleached, which indicates an effective doping process. As shown in Fig. 4, the intensity of peak at 413 nm in TCE is higher than that in CB indicating more dopant anion in the doing process. We tested the solubility of F4TCNQ in TCE and CB, as shown in Fig. S2 (in ESI). The solubility of F4TCNQ in TCE is 1.455 mg/mL which is higher than 0.434 mg/mL in CB. The higher solubility of dopants will help to increase of doping conductivity.[41]

In order to deeply explore the influence of solution state on the morphology of doped films, Cryo-SEM experiments of P3HT solution with dopant concentrations of 0 wt% and 20 wt% were performed. The results of Cryo-SEM experiments are presented in Fig. 5. It is clear that there are lots of P3HT nanofibers in TCE but no characteristic morphology in CB as shown in Fig. 5(a) and Fig. 5(c), respectively. After adding with F4TCNQ, the nanostructure of P3HT in TCE is basically kept. The nanowires in TCE solution can keep upon F4TCNQ doping. While in the CB solution, after doping with F4TCNQ, there are many disorder aggregates without good connection.

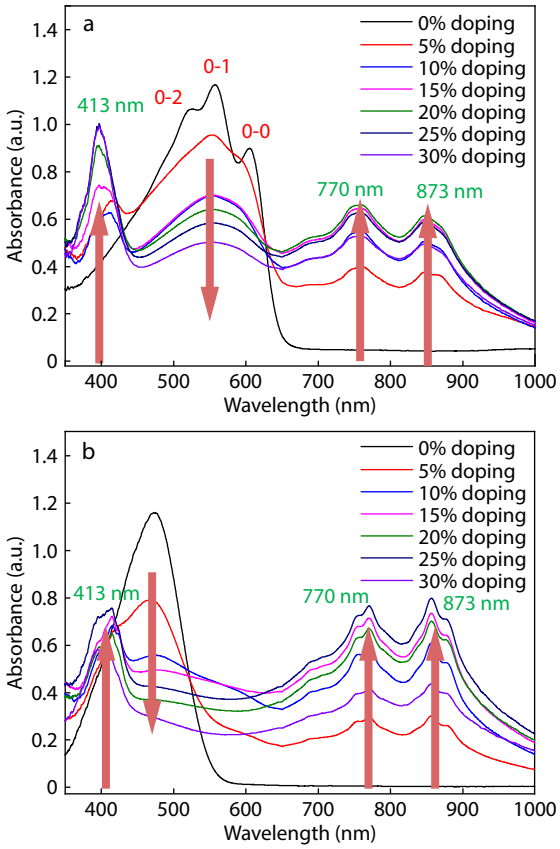

Fig. 4 UV-Vis-NIR absorbance spectra of doping solution with different dopant loading in (a) TCE and (b) CB at room temperature.

https://doi.org/10.1007/s10118-023-2939-x

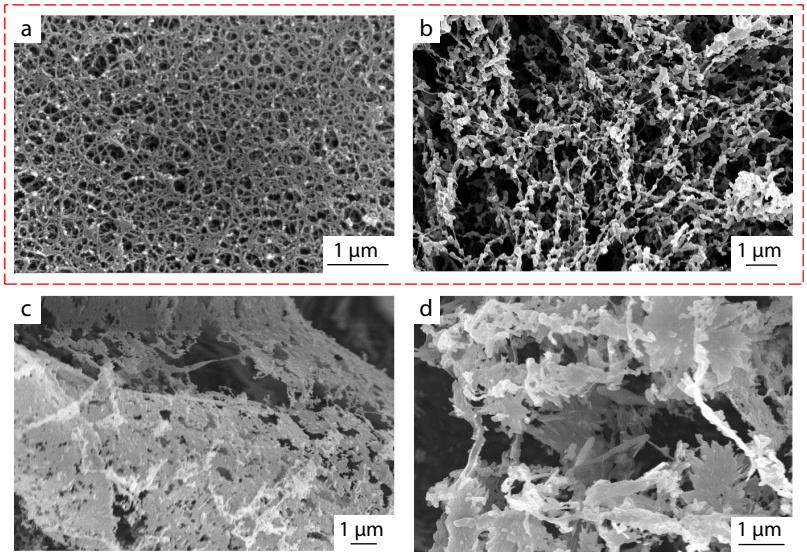

Fig. 5 Cryo-SEM images of pristine P3HT solution from (a) TCE and (c) CB, and doped P3HT solution from (b) TCE and (d) CB. For doped P3HT solution, the dopant F4TCNQ concentration is 20 wt%.

Distribution of F4TCNQ in the P3HT Films

To investigate structural differences at the molecular level between F4TCNQ-doped P3HT films processed from solvent TCE and solvent CB, we performed a series of out-of-plane GIXRD and in-plane GIXRD measurements, TEM and FTIR spectra with different F4TCNQ concentration. The whole out-of-plane GIXRD patterns including lamellar (100), (200), (300) and (010) π-stacking peak of P3HT are shown in Fig. S3 (in ESI). In order to observe the peak in out-of-plane GIXRD pattern more clearly, only the region of 2θ between 3.2° and 8° was selected and the peak was normalized to the max intensity. Fig. 6 shows a gradual change of the out-of-plane lamellar structure of doped P3HT film processed from solvent TCE and solvent CB as the doping level is increased. In this 2θ region, there is only one peak corresponding to P3HT lamellar (100) peak can be observed.[42–45] For the undoped P3HT films, the (100) peak at the same position for TCE and CB, and the lamellar spacing is 1.62 nm. With the addition of F4TCNQ, the (100) peak gradually moves to lower 2θ and that means the lamellar spacing of P3HT increases in both solvent TCE and CB. The reason for swelling lamellar spacing is that the F4TCNQ counteranion locates in the lamellar region of the P3HT crystallites.[46–48]

Although the same trend of lamellar spacing in solvent TCE and CB is observed, there are still lots of differences which indicate the different way F4TCNQ interacting with P3HT between solvent TCE and CB. At 5 wt% dopant loading, the (100) peak for solvent CB moves only slowly to low 2θ and the situation is very different in solvent TCE which has an obvious change. As a result, the lamellar spacing is 1.78 and 1.68 nm in solvent TCE and CB, respectively. The polymer chain in solvent CB is random coil conformation and this needs more energy to drive the doping process between F4TCNQ and P3HT. Thus, at the low dopant concentration, there is a small doping effect in solvent CB and causes no obvious (100) peak shifting. In the solvent TCE, P3HT aggregates have a favorable doping effect and the F4TCNQ almost doping with P3HT chain which causes obvious (100) peak shifting. The specific value of lamellar spacing of doped P3HT with different dopant concentrations is listed in Table 1. At the high dopant concentration (dopant loading content more than 10 wt%), the lamellar distance of doped P3HT from TCE is smaller than CB, which means a tighter crystal in TCE. The smaller lamellar distance is also an indication of a more ordered structure in doped polymer films.[49,50]

However, the π-π stacking or (010) diffraction peak observed in the in-plane direction showed different changing between TCE and CB. Fig. 6(c) shows the change of the in-plane π-π structure of doped P3HT film processed from solvent TCE and Fig. 6(d) shows the change from solvent CB as the doping level increasing. In TCE, after doping with F4TCNQ, the (010) diffraction peak moved to higher θ, indicating a decrease of π-π stacking distance. In this situation, the doping induced polaron delocalizes between adjacent chains and thus leads to an stronger attractive forces which reduce the π-π distance of polymer.[51] However, in CB, after doping with F4TCNQ, the (010) diffraction peak was splitted into two peaks. One moved to higher theta, indicating a decrease of π-π stacking distance and one moved to lower theta, indicating an increase of π-π stacking distance. Only the dopants which enter the π-π stacking region of polymer and form a new crystalline phase will expand the π-π stacking distance. The specific values of π-π distance from solvent TCE and CB are listed in Table 1. In TCE solution doping, the dopant only entered the alkyl side chain region of the polymer and hardly entered the π-π stacking region of polymer because polymer chain crystallization by strong π-π interaction and the unfavorable interaction between polymer chain and solvent. However, in CB solution doping, P3HT with a disordered coil conformation, it is easy for the dopant enters both the alkyl side chain region of the polymer and the π-π stacking region.

The change of lamellar distance and π-π distance of doped P3HT with different dopant concentrations are represented in Figs. 7(a) and 7(b) according to the out-of-plane and in-plane GIXRD results. In solvent TCE doping, dopants only enter the lamellar region of P3HT which drive the phase transition and

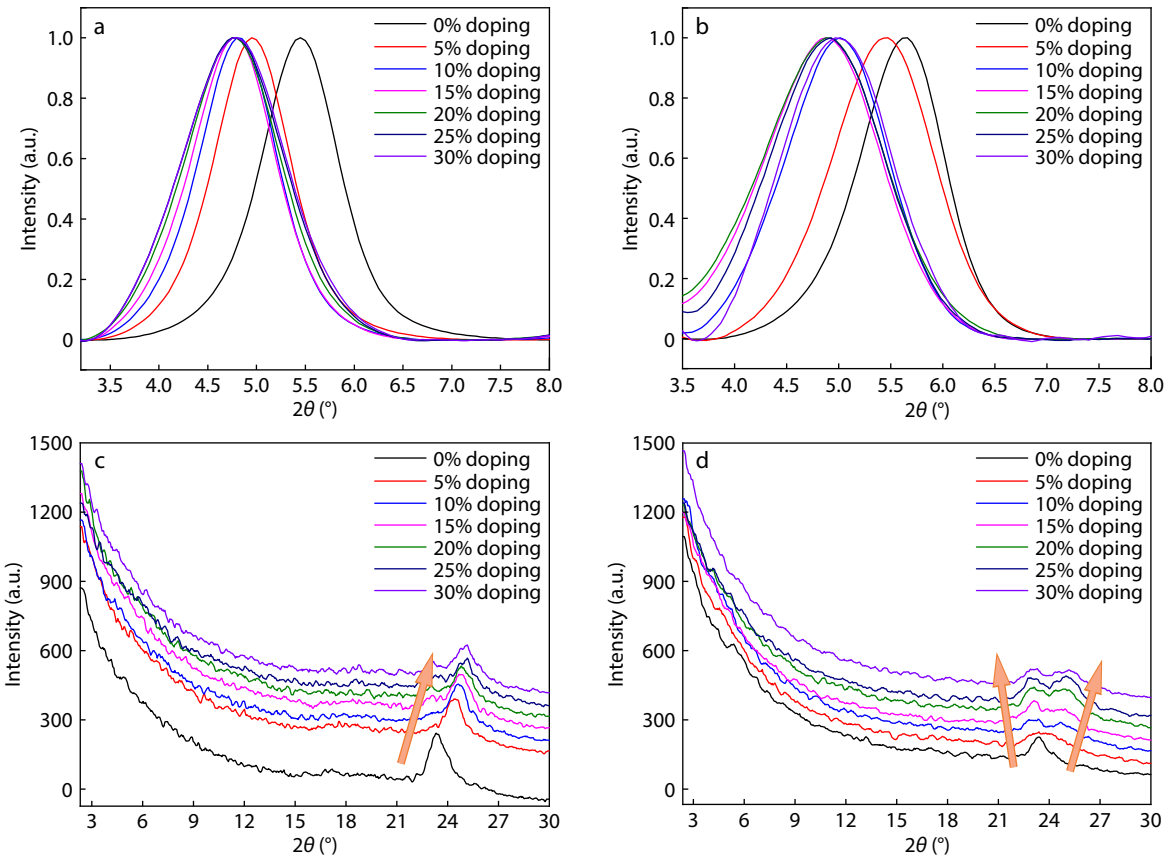

Fig. 6 Out-of-plane GIXD of pristine and doped P3HT from (a) TCE and (b) CB and in-plane GIXD of pristine and doped P3HT from (c) TCE and (d) CB. The 2θ of out-of-plane GIXD ranging from 3.2° to 8.0°, the 2θ of in-plane GIXD ranging from 2° to 30°.

Table 1 The lamellar distance and π-π distance of doped P3HT calculating from out-of-plane GIXD and in-plane GIXD processed from different solvents.

Dopant concentration (wt%)	TCE		CB	
	Lamellar distance (nm)	π-π Distance (Å)	Lamellar distance (nm)	π-π Distance (Å)
0	1.62	3.82	1.62	3.81
5	1.78	3.66	1.68	3.78
10	1.84	3.62	1.86	3.62 3.86
15	1.84	3.60	1.92	3.60 3.86
20	1.86	3.60	1.92	3.60 3.88
25	1.86	3.54	1.90	3.57 3.88
30	1.84	3.54	1.88	3.55 3.88

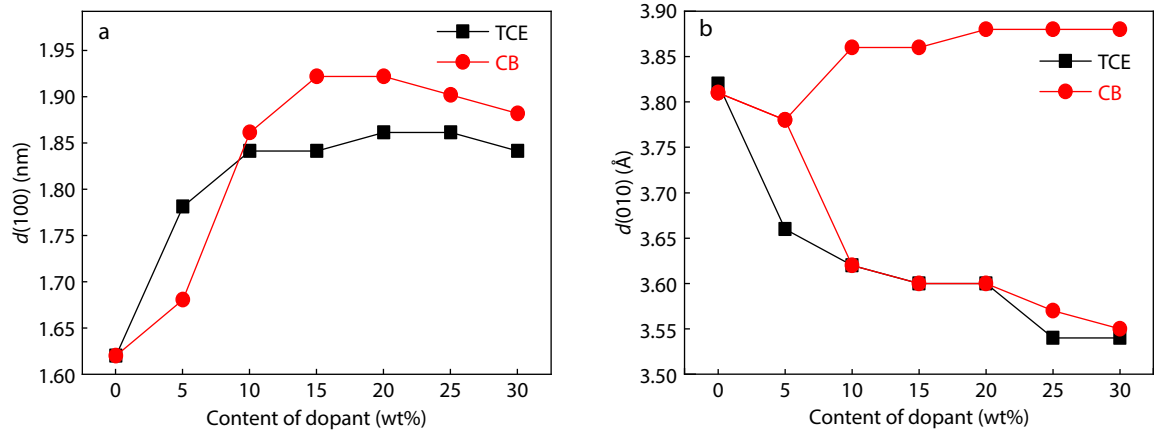

Fig. 7 (a) The lamellar distance and (b) π-π distance of doped P3HT from different solvents.

https://doi.org/10.1007/s10118-023-2939-x

lamellar spacing expansion. However, in solvent CB doping, dopants interact with the side chain and backbone of polymer which cause both lamellar spacing and π-π stacking distance to increase. The decrease of π-π stacking distance in both TCE and CB is likely the result of polaron delocalization.

2D-GIWAXS characterization of the doped P3HT films was also performed to detect the change of crystallinity and orientation.[52–54] The 2D-GIWAXS patterns of all different dopant concentrations are shown in Fig. S4 (in ESI). Here, we choose the dopant concentration of 0 wt% and 20 wt% to discuss the structure of doped film as shown in Fig. 8. The films processed TCE have obvious (100), (200) and (300) diffraction peaks in the out of plane and one (010) diffraction peak in plane. From 0 wt% to 20 wt% dopant concentration, the characteristic is not changed which indicating the keeping of edge-on orientation upon doping process. However, in CB doping, the films have only (100) diffraction peak in the out of plane and the double (010) diffraction peak in plane indicating of structure change and the loss of edge-on orientation. The intensity of 2D-GIWAXS patterns is larger in TCE than that in CB which is the result of higher crystallinity processed from TCE.

We performed TEM imaging of pristine and doped P3HT films to evaluate the morphology changing of P3HT after doping with F4TCNQ as shown in Fig. 9. The TEM imaging of pristine and doped P3HT shows similar behavior with Cryo-SEM images in Fig. 5. The pristine film of P3HT processed from TCE covered with dense fibers. With the increasing content of F4TCNQ, the fiber network in P3HT film was still maintained. The fiber long axis was the π-π packing direction of the polymer chain and the fiber was not damaged, indicating that there was not a large amount of F4TCNQ entering the π-π region of the polymer, which was also consistent with our observation in in-plane GIXRD. A large number of fibers in the doped film also ensured the polaron (bipolaron) on the polymer chain transport rapidly and continuously, which ultimately improved the conductivity.[55–57] The pristine film of P3HT processed from CB was uniform as shown in Fig. 9(b). When a small amount of F4TCNQ was added, the P3HT film can barely maintain uniform morphology. With the increase of dopant content, large disordered aggregates appeared in the film. This result consists with previous studies that when P3HT was dissolved in good solvent CB, the addition of F4TCNQ will rapidly promote the aggregation of the polymer, and finally led to poor morphology.[4,13,20] The discontinuous disordered aggregates localized polaron (bipolaron) and limited transport over long distance.

To compare the difference in doping efficiency of films cast from solvent TCE and CB, the FTIR spectra were characterized as shown in Fig. 10. The vibration absorption band of cyano-group on dopant molecule is closely related to its charge state, which makes it possible to use FTIR to study the doping process.[58–60] The vibration frequency of cyano-group on the neutral F4TCNQ is 2227 cm^{-1}. When F4TCNQ receives the

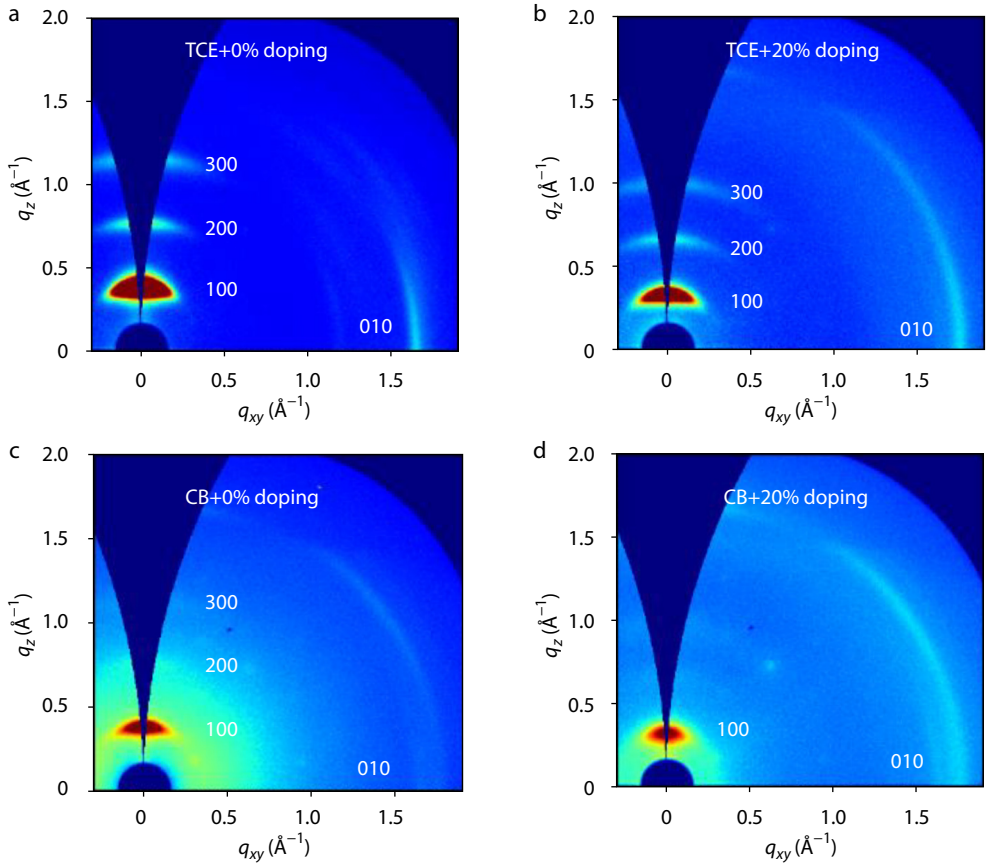

Fig. 8 GIWAXS of (a) pristine P3HT film processed from solvent TCE, (b) doped P3HT film processed from solvent TCE, (c) pristine P3HT film processed from solvent CB and (d) doped P3HT film processed from solvent CB.

https://doi.org/10.1007/s10118-023-2939-x

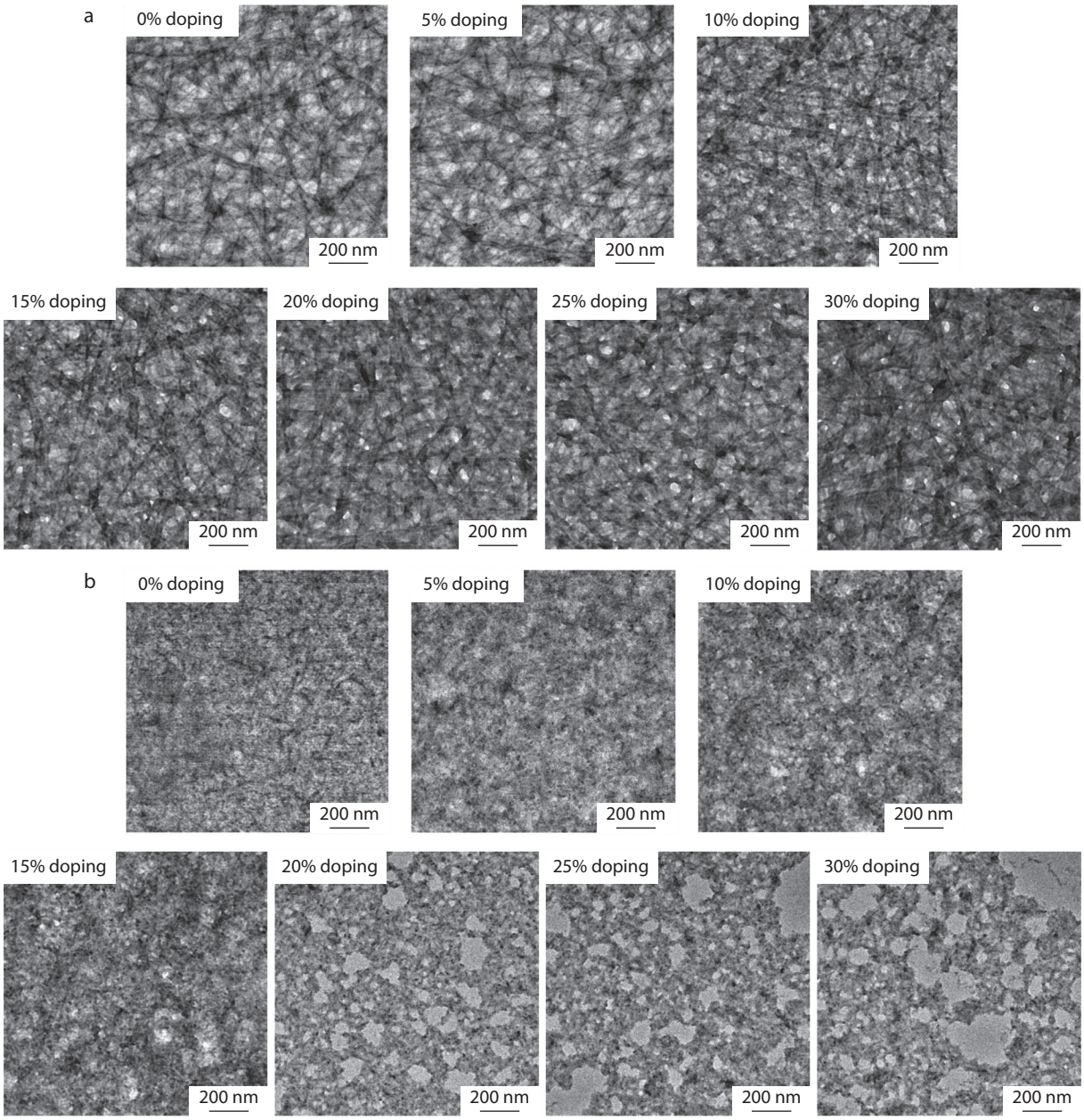

Fig. 9 TEM images of pristine and doped P3HT (F4TCNQ concentrations: 5%, 10%, 15%, 20%, 25% and 30%) from solvent (a) TCE and (b) CB. The magnification of the images was 25000×.

electrons from the polymer, the vibration absorption band moves to the direction of low energy, and the degree of shifting is positively correlated with the degree of accepting electrons.[12] Fig. 10(a) is the FTIR data of doped P3HT films from solvent TCE with different dopant concentrations and the wave number range is between 2140 and 2260 cm^{-1} without the interference from other vibration bands. The vibration absorption band stays at 2188/2169 cm^{-1} and does not move with the increase of doping concentration. When processing from solvent CB, the band changes to 2194/2169 cm^{-1} and still remains stay with increasing dopant concentration, as shown in Fig. 10(b). However, the vibration absorption peak of cyano-group in TCE is redshifted by 6 cm^{-1} than that in CB, indicating a higher degree of charge transfer and a higher doping efficiency in the film from TCE. Fig. 10(c) is the FTIR data of doped P3HT films from solvent TCE and CB with 20% dopant concentration and the energy range is between 0.05 and 0.75 eV. After doping with F4TCNQ, strong vibration absorption peaks appear below 0.2 eV, and a broad absorption peak is related to the degree of delocalization of charge in the polymer backbone.[61–63] At the 20% dopant concentration, P1 absorption peak in TCE is at 0.52 eV, while P1 absorption peak in CB is at 0.54 eV, with a red-shift of 0.02 eV. This indicates the polaron in TCE has a higher degree of delocalization, which is conducive to improving the conductivity.

The film obtained by doping P3HT in the random coil state

https://doi.org/10.1007/s10118-023-2939-x

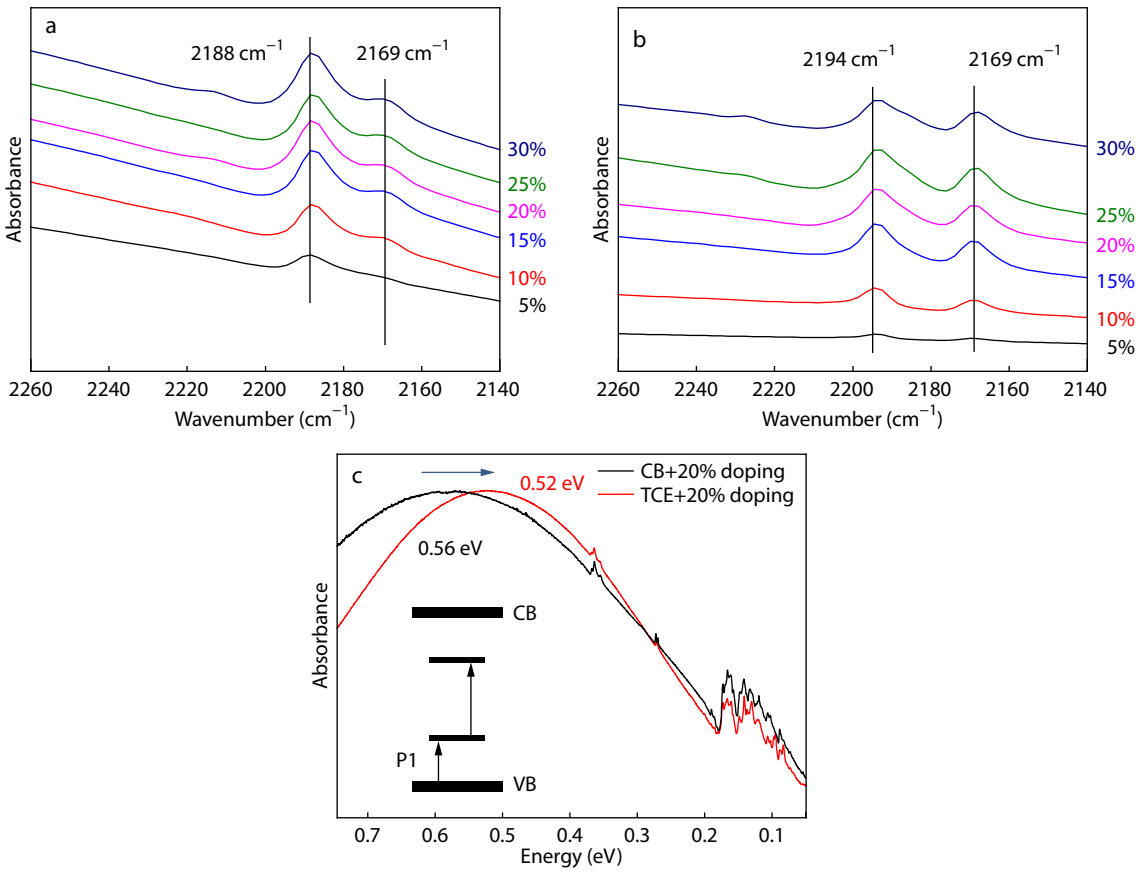

Fig. 10 FTIR spectra in the characteristic cyano-group stretching region of increasingly doped P3HT films from solvent (a) TCE and (b) CB; (c) P1 peak of doped P3HT from TCE and CB in IR region.

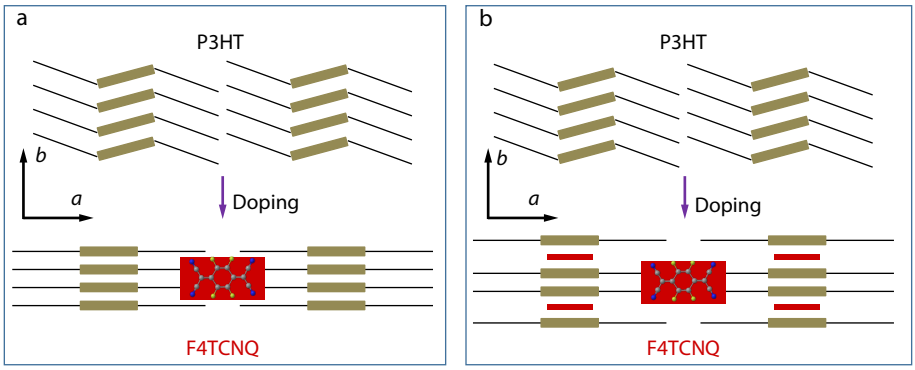

Fig. 11 Schematic illustrations of the distribution of F4TCNQ in P3HT thin film obtained from (a) TCE and (b) CB solution.

in CB has low crystallinity and ordering, and F4TCNQ is disorderly distributed in the alkyl side chain region of the polymer and π-π stacking region of polymer. However, the film obtained by doping P3HT crystallized in TCE has higher ordering and crystallinity. F4TCNQ is only distributed in the alkyl side chain region of the polymer, as shown in Fig. 11. In the marginal solvent, P3HT will form lots of crystallites by favor π-π interaction between the backbone. The HOMO level of crystalline region is higher than that in amorphous region which is beneficial to the doping process and the large of lamellar region can accommodate lots of dopants. And the flexible alkyl side chains have plenty of entropy for disturbance, so it is easy for F4TCNQ to enter the lamellar spacing compared to the polymer π stacks. While in good solvent, P3HT has a random coil conformation, after adding with dopants, F4TCNQ interacts with polymer chain intimately. The strong interaction causes dopants distribute disorderly in the crystalline region, amorphous region, π-π region and lamellar region of polymer film. The dopant anion in the π-π region has a strong coulomb interaction with the polaron on the backbone produced by doping, which is not conducive to delocalization and effective transport of polaron. However, dopants only distributed in the alkyl side chain region of the polymer have spatial separation from backbone which is beneficial to form ICT state and improve doping efficiency. Meanwhile, due to the higher solubility of dopant F4TCNQ in TCE, most dopants

https://doi.org/10.1007/s10118-023-2939-x

are in a dispersed state and have doping effect with the polymer, while more neutral state F4TCNQ is retained in the film which does not have doping effect with the polymer when processed from CB. The higher crystallinity in TCE is also help to increase electrical conductivity.

CONCLUSIONS

By regulating the aggregation states of P3HT in different kinds of solvents by cooling it from higher temperature to room temperature, we obtained two different doping stacking structures. When the P3HT aggregates in TCE was doped, the dopant only entered the alkyl side chain region of the polymer. However, when doping P3HT with a disordered coil conformation in CB, the dopant enters both the alkyl side chain region of the polymer and the *π*-*π* stacking region. For the doping of P3HT in TCE solution, the dopants did not destroy the *π*-*π* interaction between polymer chains which guarantees the high crystallinity of polymer. The dopants located in the alkyl side chain region has smaller Coulomb interaction to the polarons on polymer chain, which is beneficial for the dissociation and transport of charge. Meanwhile, due to the higher solubility of dopant in TCE, TCE has more anion dopant in the doped film, indicating that there are more polarons in the polymer. So that it has higher conductivity (23 S/cm) in TCE than that doping P3HT with a disordered coil conformation in CB (7 S/cm).

NOTES

The authors declare no competing financial interest.

Electronic Supplementary Information

Electronic supplementary information (ESI) is available free of charge in the online version of this article at http://doi.org/10.1007/s10118-023-2939-x.

ACKNOWLEDGMENTS

This work was financially supported by the National Natural Science Foundation of China (No. 51933010). We also thank Beijing Synchrotron Radiation Facility (BSRF) 1W1A.

REFERENCES

1 Jacobs, I. E.; Moule, A. J. Controlling molecular doping in organic semiconductors. *Adv. Mater.* **2017**, *29*, 1703063.
2 Scaccabarozzi, A. D.; Basu, A.; Anies, F.; Liu, J.; Zapata-Arteaga, O.; Warren, R.; Firdaus, Y.; Nugraha, M. I.; Lin, Y. B.; Campoy-Quiles, M.; Koch, N.; Muller, C.; Tsetseris, L.; Heeney, M.; Anthopoulos, T. D. Doping approaches for organic semiconductors. *Chem. Rev.* **2022**, *122*, 4420–4492.
3 Pingel, P.; Neher, D. Comprehensive picture of p-type doping of P3HT with the molecular acceptor F(4)TCNQ. *Phys. Rev. B* **2013**, *87*, 115209.
4 Scholes, D. T.; Hawks, S. A.; Yee, P. Y.; Wu, H.; Lindemuth, J. R.; Tolbert, S. H.; Schwartz, B. J. Overcoming film quality issues for conjugated polymers doped with F(4)TCNQ by solution sequential processing: hall effect, structural, and optical measurements. *J. Phys. Chem. Lett.* **2015**, *6*, 4786–4793.
5 Hynynen, J.; Kiefer, D.; Yu, L.; Kroon, R.; Munir, R.; Amassian, A.; Kemerink, M.; Müller, C. Enhanced electrical conductivity of molecularly p-doped poly(3-hexylthiophene) through understanding the correlation with solid-state order. *Macromolecules* **2017**, *50*, 8140–8148.
6 Lim, E.; Peterson, K. A.; Su, G. M.; Chabinyc, M. L. Thermoelectric properties of poly(3-hexylthiophene) (P3HT) doped with 2,3,5,6-tetrafluoro-7,7,8,8-tetracyanoquinodimethane (F4TCNQ) by vapor-phase infiltration. *Chem. Mater.* **2018**, *30*, 998–1010.
7 Untilova, V.; Biskup, T.; Biniek, L.; Vijayakumar, V.; Brinkmann, M. Control of chain alignment and crystallization helps enhance charge conductivities and thermoelectric power factors in sequentially doped P3HT:F-4TCNQ films. *Macromolecules* **2020**, *53*, 2441–2453.
8 Gao, J.; Niles, E. T.; Grey, J. K. Aggregates promote efficient charge transfer doping of poly(3-hexylthiophene). *J. Phys. Chem. Lett.* **2013**, *4*, 2953–2957.
9 Zhou, Y. Y.; Wang, Z. Y.; Yao, Z. F.; Yu, Z. D.; Lu, Y.; Wang, X. Y.; Liu, Y.; Li, Q. Y.; Zou, L.; Wang, J. Y.; Pei, J. Systematic investigation of solution-state aggregation effect on electrical conductivity in doped conjugated polymers. *CCS Chem.* **2021**, *3*, 2994–3004.
10 Yim, K. H.; Whiting, G. L.; Murphy, C. E.; Halls, J. J. M.; Burroughes, J. H.; Friend, R. H.; Kim, J. S. Controlling electrical properties of conjugated polymers *via* a solution-based p-type doping. *Adv. Mater.* **2008**, *20*, 3319–3324.
11 Duong, D. T.; Wang, C. C.; Antono, E.; Toney, M. F.; Salleo, A. The chemical and structural origin of efficient p-type doping in P3HT. *Org. Electron.* **2013**, *14*, 1330–1336.
12 Méndez, H.; Heimel, G.; Winkler, S.; Frisch, J.; Opitz, A.; Sauer, K.; Wegner, B.; Oehzelt, M.; Röthel, C.; Duhm, S.; Többens, D.; Koch, N.; Salzmann, I. Charge-transfer crystallites as molecular electrical dopants. *Nat. Commun.* **2015**, *6*, 8560.
13 Jacobs, I. E.; Aasen, E. W.; Oliveira, J. L.; Fonseca, T. N.; Roehling, J. D.; Li, J.; Zhang, G. W.; Augustine, M. P.; Mascal, M.; Moule, A. J. Comparison of solution-mixed and sequentially processed P3HT:F4TCNQ films: effect of doping-induced aggregation on film morphology. *J. Mater. Chem. C* **2016**, *4*, 3454–3466.
14 Hamidi-Sakr, A.; Biniek, L.; Bantignies, J. L.; Maurin, D.; Herrmann, L.; Leclerc, N.; Leveque, P.; Vijayakumar, V.; Zimmermann, N.; Brinkmann, M. A versatile method to fabricate highly in-plane aligned conducting polymer films with anisotropic charge transport and thermoelectric properties: the key role of alkyl side chain layers on the doping mechanism. *Adv. Funct. Mater.* **2017**, *27*, 1700173.
15 Yan, H.; Ma, W. Molecular doping efficiency in organic semiconductors: fundamental principle and promotion strategy. *Adv. Funct. Mater.* **2022**, *32*, 2111351.
16 Jacobs, I. E.; Cendra, C.; Harrelson, T. F.; Valdez, Z. I. B.; Faller, R.; Salleo, A.; Moule, A. J. Polymorphism controls the degree of charge transfer in a molecularly doped semiconducting polymer. *Mater. Horiz.* **2018**, *5*, 655–660.
17 Neelamraju, B.; Watts, K. E.; Pemberton, J. E.; Ratcliff, E. L. Correlation of coexistent charge transfer states in F(4)TCNQ-doped P3HT with microstructure. *J. Phys. Chem. Lett.* **2018**, *9*, 6871–6877.
18 Wu, E. C. K.; Salamat, C. Z.; Tolbert, S. H.; Schwartz, B. J. Molecular dynamics study of the thermodynamics of integer charge transfer vs charge-transfer complex formation in doped conjugated polymers. *ACS Appl. Mater. Interfaces* **2022**, *14*, 26988–27001.
19 Stanfield, D. A.; Wu, Y. T.; Tolbert, S. H.; Schwartz, B. J. Controlling the formation of charge transfer complexes in chemically doped semiconducting polymers. *Chem. Mater.* **2021**, *33*, 2343–2356.

20 McFarland, F. M.; Ellis, C. M.; Guo, S. The aggregation of poly(3-hexylthiophene) into nanowires: with and without chemical doping. *J. Phys. Chem. C* **2017**, *121*, 4740–4746.
21 McFarland, F. M.; Bonnette, L. R.; Acres, E. A.; Guo, S. The impact of aggregation on the p-doping kinetics of poly(3-hexylthiophene). *J. Mater. Chem. C* **2017**, *5*, 5764–5771.
22 Tang, K.; McFarland, F. M.; Travis, S.; Lim, J.; Azoulay, J. D.; Guo, S. Aggregation of P3HT as a preferred pathway for its chemical doping with F-4-TCNQ. *Chem. Commun.* **2018**, *54*, 11925–11928.
23 Gao, J.; Stein, B. W.; Thomas, A. K.; Garcia, J. A.; Yang, J.; Kirk, M. L.; Grey, J. K. Enhanced charge transfer doping efficiency in J-aggregate poly(3-hexylthiophene) nanofibers. *J. Phys. Chem. C* **2015**, *119*, 16396–16402.
24 Wang, C. C.; Duong, D. T.; Vandewal, K.; Rivnay, J.; Salleo, A. Optical measurement of doping efficiency in poly(3-hexylthiophene) solutions and thin films. *Phys. Rev. B* **2015**, *91*, 085205.
25 Harrelson, T. F.; Cheng, Y. Q. Q.; Li, J.; Jacobs, I. E.; Ramirez-Cuesta, A. J.; Faller, R.; Moule, A. J. Identifying atomic scale structure in undoped/doped semicrystalline P3HT using inelastic neutron scattering. *Macromolecules* **2017**, *50*, 2424–2435.
26 Chen, L.; Wang, H. Y.; Liu, J. G.; Xing, R. B.; Yu, X. H.; Han, Y. C. Tuning the pi-pi stacking distance and J-aggregation of DPP-based conjugated polymer *via* introducing insulating polymer. *J. Polym. Sci., Part B: Polym. Phys.* **2016**, *54*, 838–847.
27 Tsoi, W. C.; Spencer, S. J.; Yang, L.; Ballantyne, A. M.; Nicholson, P. G.; Turnbull, A.; Shard, A. G.; Murphy, C. E.; Bradley, D. D. C.; Nelson, J.; Kim, J. S. Effect of crystallization on the electronic energy levels and thin film morphology of P3HT:PCBM blends. *Macromolecules* **2011**, *44*, 2944–2952.
28 Gao, W. Y.; Kahn, A. Controlled p-doping of zinc phthalocyanine by coevaporation with tetrafluorotetracyanoquinodimethane: a direct and inverse photoemission study. *Appl. Phys. Lett.* **2001**, *79*, 4040–4042.
29 Yoon, S. E.; Kang, Y.; Jeon, G. G.; Jeon, D.; Lee, S. Y.; Ko, S. J.; Kim, T.; Seo, H.; Kim, B. G.; Kim, J. H. Exploring wholly doped conjugated polymer films based on hybrid doping: strategic approach for optimizing electrical conductivity and related thermoelectric properties. *Adv. Funct. Mater.* **2020**, *30*, 2004598.
30 Muller, L.; Nanova, D.; Glaser, T.; Beck, S.; Pucci, A.; Kast, A. K.; Schroder, R. R.; Mankel, E.; Pingel, P.; Neher, D.; Kowalsky, W.; Lovrincic, R. Charge-transfer-solvent interaction predefines doping efficiency in p-doped P3HT films. *Chem. Mater.* **2016**, *28*, 4432–4439.
31 Duong, D. T.; Phan, H.; Hanifi, D.; Jo, P. S.; Nguyen, T. Q.; Salleo, A. Direct observation of doping sites in temperature-controlled, p-doped P3HT thin films by conducting atomic force microscopy. *Adv. Mater.* **2014**, *26*, 6069–6073.
32 Hase, H.; O'Neill, K.; Frisch, J.; Opitz, A.; Koch, N.; Salzmann, I. Unraveling the microstructure of molecularly doped poly(3-hexylthiophene) by thermally induced dedoping. *J. Phys. Chem. C* **2018**, *122*, 25893–25899.
33 Aziz, E. E.; Vollmer, A.; Eisebitt, S.; Eberhardt, W.; Pingel, P.; Neher, D.; Koch, N. Localized charge transfer in a molecularly doped conducting polymer. *Adv. Mater.* **2007**, *19*, 3257–3260.
34 Liao, Z. X.; Wang, S. C.; Gao, C. M.; Wang, L. Combining chemical doping and thermal annealing to optimize the thermoelectric performance of the poly(3-hexylthiophene). *Compos. Commun.* **2022**, *34*, 101255.
35 Zhao, K. F.; Zhang, Q.; Chen, L.; Zhang, T.; Han, Y. C. Nucleation and growth of P(NDI2OD-T2) nanowires *via* side chain ordering and backbone planarization. *Macromolecules* **2021**, *54*, 2143–2154.
36 Li, H. X.; Yang, H.; Zhang, L.; Wang, S. C.; Chen, Y.; Zhang, Q.; Zhang, J. D.; Tian, H. K.; Han, Y. C. Optimizing the crystallization behavior and film morphology of donor-acceptor conjugated semiconducting polymers by side-chain-solvent interaction in nonpolar solvents. *Macromolecules* **2021**, *54*, 10557–10573.
37 Zhao, K.; Xue, L. J.; Liu, J. G.; Gao, X.; Wu, S. P.; Han, Y. C.; Geng, Y. H. A new method to improve poly(3-hexyl thiophene) (P3HT) crystalline behavior: decreasing chains entanglement to promote order-disorder transformation in solution. *Langmuir* **2010**, *26*, 471–477.
38 Zhang, R.; Yang, H.; Zhou, K.; Zhang, J. D.; Yu, X. H.; Liu, J. G.; Han, Y. C. Molecular orientation and phase separation by controlling chain segment and molecule movement in P3HT/N2200 blends. *Macromolecules* **2016**, *49*, 6987–6996.
39 Sun, Y.; Liu, J. G.; Ding, Y.; Han, Y. C. Controlling the surface composition of PCBM in P3HT/PCBM blend films by using mixed solvents with different evaporation rates. *Chinese J. Polym. Sci.* **2013**, *31*, 1029–1037.
40 Barrett, B. J.; Saund, S. S.; Dziatko, R. A.; Clark-Winters, T. L.; Katz, H. E.; Bragg, A. E. Spectroscopic studies of charge-transfer character and photoresponses of F4TCNQ-based donor-acceptor complexes. *J. Phys. Chem. C* **2020**, *124*, 9191–9202.
41 Li, J.; Zhang, G. W.; Holm, D. M.; Jacobs, I. E.; Yin, B.; Stroeve, P.; Mascal, M.; Moule, A. J. Introducing solubility control for improved organic P-type dopants. *Chem. Mater.* **2015**, *27*, 5765–5774.
42 Liu, J. G.; Sun, Y.; Zheng, L. D.; Geng, Y. H.; Han, Y. C. Vapor-assisted imprinting to pattern poly(3-hexylthiophene) (P3HT) film with oriented arrangement of nanofibrils and flat-on conformation of P3HT chains. *Polymer* **2013**, *54*, 423–430.
43 Xu, Y. Z.; Liu, J. G.; Wang, H. Y.; Han, Y. C. Hierarchical network-like structure of poly(3-hexlthiophene) (P3HT) by accelerating the disentanglement of P3HT in a P3HT/PS (polystyrene) blend. *RSC Adv.* **2013**, *3*, 17195–17202.
44 Zhang, R.; Yan, Y.; Yang, H.; Yu, X. H.; Liu, J. G.; Zhang, J. D.; Han, Y. C. The broken out and confinement phase separation structure evolution with the solution aggregation and relative crystallization degree in P3HT/N2200. *Polymer* **2018**, *138*, 49–56.
45 Liang, Q. J.; Jiao, X. C.; Yan, Y.; Xie, Z. Y.; Lu, G. H.; Liu, J. G.; Han, Y. C. Separating crystallization process of P3HT and O-IDTBR to construct highly crystalline interpenetrating network with optimized vertical phase separation. *Adv. Funct. Mater.* **2019**, *29*, 1807591.
46 Patel, S. N.; Glaudell, A. M.; Peterson, K. A.; Thomas, E. M.; O'Hara, K. A.; Lim, E.; Chabinyc, M. L. Morphology controls the thermoelectric power factor of a doped semiconducting polymer. *Sci. Adv.* **2017**, *3*, e1700434.
47 Vijayakumar, V.; Zaborova, E.; Biniek, L.; Zeng, H. Y.; Herrmann, L.; Carvalho, A.; Boyron, O.; Leclerc, N.; Brinkmann, M. Effect of alkyl side chain length on doping kinetics, thermopower, and charge transport properties in highly oriented F(4)TCNQ-Doped PBTTT Films. *ACS Appl. Mater. Interfaces* **2019**, *11*, 4942–4953.
48 Tanaka, H.; Kanahashi, K.; Takekoshi, N.; Mada, H.; Ito, H.; Shimoi, Y.; Ohta, H.; Takenobu, T. Thermoelectric properties of a semicrystalline polymer doped beyond the insulator-to-metal transition by electrolyte gating. *Sci. Adv.* **2020**, *6*, eaay8065.
49 Zhou, K.; Liu, J. G.; Zhang, R.; Zhao, Q. Q.; Cao, X. X.; Yu, X. H.; Xing, R. B.; Han, Y. C. The molecular regioregularity induced morphological evolution of polymer blend thin films. *Polymer* **2016**, *86*, 105–112.
50 Chen, L.; Zhao, K. F.; Chi, S. J.; Liu, J. G.; Yu, X. H.; Han, Y. C. Improving fiber alignment by increasing the planar conformation of isoindigo-based conjugated polymers. *Mater. Chem. Front.* **2017**, *1*, 286–293.
51 Liu, W.; Müller, L.; Ma, S.; Barlow, S.; Marder, S. R.; Kowalsky, W.; Köhn, A.; Lovrincic, R. Origin of the π-π spacing change upon doping of semiconducting polymers. *J. Phys. Chem. C* **2018**, *122*,

27983–27990.
52 Chen, W. C.; Xiao, M. J.; Yang, C. P.; Duan, L. R.; Yang, R. Q. Efficient P3HT:PC61BM solar cells employing 1,2,4-trichlorobenzene as the processing additives. *Chinese J. Polym. Sci.* **2017**, *35*, 302–308.
53 Chu, X.; Kang, J. Q.; Hong, Y.; Zhu, G. D.; Yan, S. K.; Wang, X. Y.; Sun, X. L. The effect of substrate on the properties of non-volatile ferroelectric P(VDF-TrFE)/P3HT Memory Devices. *Chinese J. Polym. Sci.* **2022**, *40*, 692–699.
54 Qiao, X. L.; Yang, J.; Han, L. H.; Zhang, J. D.; Zhu, M. F. Synergistic effects of solvent vapor assisted spin-coating and thermal annealing on enhancing the carrier mobility of poly(3-hexylthiophene) field-effect transistors. *Chinese J. Polym. Sci.* **2021**, *39*, 849–855.
55 Zhao, Y. F.; Zou, W. J.; Li, H.; Lu, K.; Yan, W.; Wei, Z. X. Large-area, flexible polymer solar cell based on silver nanowires as transparent electrode by roll-to-roll printing. *Chinese J. Polym. Sci.* **2017**, *35*, 261–268.
56 Xue, W.; Xu, M.; Yu, M. N.; Sun, H. M.; Lin, J. Y.; Jiang, R. C.; Xie, L. H.; Shi, N. E.; Huang, W. Electrospun supramolecular hybrid microfibers from conjugated polymers: color transformation and conductivity evolution. *Chinese J. Polym. Sci.* **2021**, *39*, 824–830.
57 Liu, Y. X.; Wang, L.; Zhou, K.; Wu, H. B.; Zhou, X. B.; Ma, Z. F.; Guo, S. W.; Ma, W. Subtle alignment of organic semiconductors at the donor/acceptor heterojunction facilitates the photoelectric conversion process. *Chinese J. Polym. Sci.* **2022**, *40*, 951–959.
58 Chappell, J. S.; Bloch, A. N.; Bryden, W. A.; Maxfield, M.; Poehler, T. O.; Cowan, D. O. Degree of charge-transfer in organic conductors by infrared-absorption spectroscopy. *J. Am. Chem. Soc.* **1981**, *103*, 2442–2443.
59 Meneghetti, M.; Pecile, C. Charge-transfer organic-crystals-molecular vibrations and spectroscopic effects of electron-molecular vibration coupling of the strong electron-acceptor TCNQF4. *J. Chem. Phys.* **1986**, *84*, 4149–4162.
60 Haworth, N. L.; Lu, J. Z.; Vo, N.; Le, T. H.; Thompson, C. D.; Bond, A. M.; Martin, L. L. Diagnosis of the redox levels of TCNQF(4) compounds using vibrational spectroscopy. *ChemPlusChem* **2014**, *79*, 962–972.
61 Ghosh, R.; Pochas, C. M.; Spano, F. C. Polaron delocalization in conjugated polymer films. *J. Phys. Chem. C* **2016**, *120*, 11394–11406.
62 Scholes, D. T.; Yee, P. Y.; Lindemuth, J. R.; Kang, H.; Onorato, J.; Ghosh, R.; Luscombe, C. K.; Spano, F. C.; Tolbert, S. H.; Schwartz, B. J. The effects of crystallinity on charge transport and the structure of sequentially processed F(4)TCNQ-doped conjugated polymer films. *Adv. Funct. Mater.* **2017**, *27*, 1702654.
63 Ghosh, R.; Chew, A. R.; Onorato, J.; Pakhnyuk, V.; Luscombe, C. K.; Salleo, A.; Spano, F. C. Spectral signatures and spatial coherence of bound and unbound polarons in P3HT films: theory versus experiment. *J. Phys. Chem. C* **2018**, *122*, 18048–18060.

https://doi.org/10.1007/s10118-023-2939-x